Title: Heisenberg Distributed Acoustic Sensing Realized on Commercial Optical Communication Terminals

Zhongwang Pang,[1,2, †] Chunyi Li,[1,2, †] Dongqi Song,[1,2] Wenlin Li,[1,2] Tong Wu,[1,2] Hao Zhu,[1,2] Peijian Sun,[1,2] and Bo Wang[1,2, *]

1. State Key Laboratory of Precision Space-time Information Sensing Technology, Department of Precision Instrument, Tsinghua University, Beijing, China, 100084

2. Key Laboratory of Photonic Control Technology (Tsinghua University), Ministry of Education, Beijing, China, 100084

†These authors contributed equally to this paper.

E-mail: bo.wang@tsinghua.edu.cn

Contents

Supplementary Figure 1: The frequency uncertainty of ~kHz-linewidth lasers and corresponding sensing spatial resolution 2

Supplementary Note 1: H-DAS performance with and without data modulation 3

Supplementary Note 2: Sensing sensitivity of H-DAS system.....5

Supplementary Note 3: Field photographs of the construction site near the high-speed railway.....7

Supplementary Note 4: Possible approaches to improve the H-DAS specification 8

Supplementary Reference 9

Supplementary Figure 1: The frequency uncertainty of ~kHz-linewidth lasers and corresponding sensing spatial resolution. a, Heterodyne spectrum between a ~1 kHz-linewidth laser and the auxiliary laser. It corresponds to a frequency uncertainty of ~425 Hz and a theoretical spatial resolution of ~63 km. **b,** Waterfall plot and the corresponding spatial resolution obtained using the ~1 kHz-linewidth laser as the sensing source. **c,** Heterodyne spectrum between a ~4 kHz-linewidth laser and the auxiliary laser. It corresponds to a frequency uncertainty of ~1699 Hz and a theoretical spatial resolution of ~15 km. **d,** Waterfall plot and the corresponding spatial resolution obtained using the ~4 kHz-linewidth laser as the sensing source. Norm. Int.: normalized intensity.

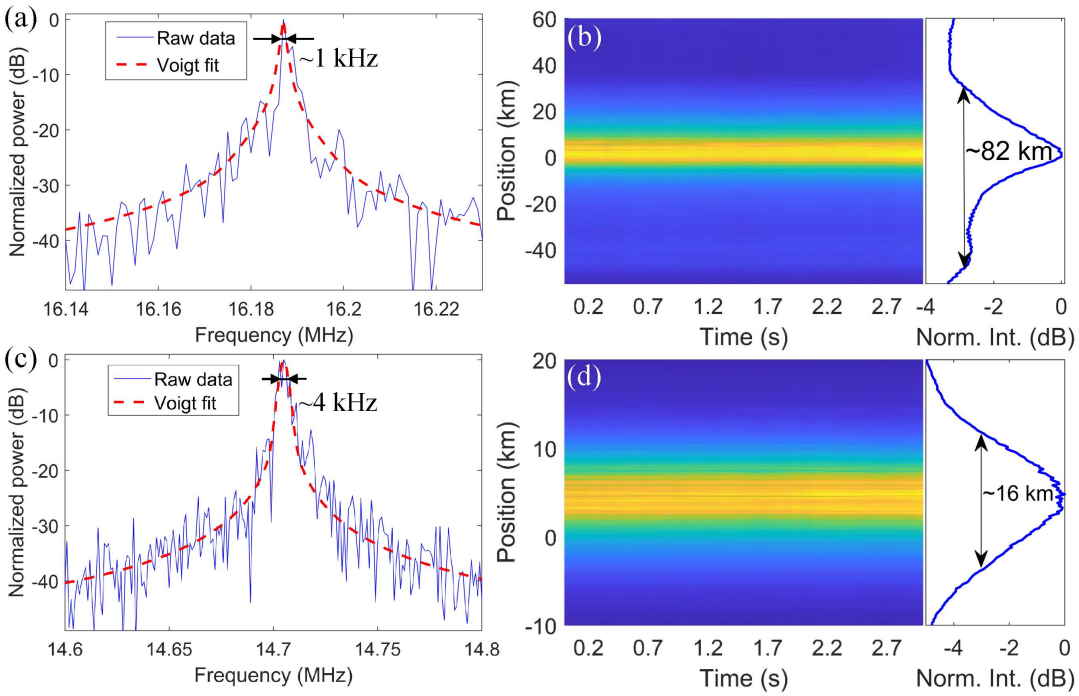

Supplementary Note 1: H-DAS performance with and without data modulation

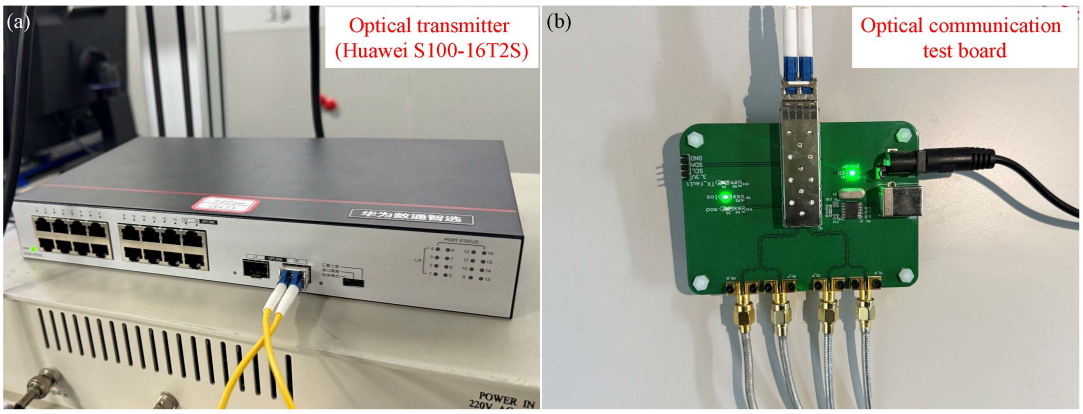

Supplementary Figure 2 | Communication hardware used in the experiments. a, Commercial optical communication terminal (Huawei S100-16T2S). **b,** Commercial optical communication test board.

In the experiments described in the main text, we achieve integrated communication and sensing using a commercial optical communication terminal, which is shown in Supplementary Fig. 2a. In normal operation, the terminal's optical output is continuously carrying Ethernet data, making it difficult to analyze the H-DAS performance when there is no data modulation. Therefore, we employ a commercial optical communication test board, as shown in Supplementary Fig. 2b. The test board operates in two modes. For mode 1, it outputs a 1.25-Gbps intensity-modulated signal. For mode 2, the data drive is turned off and the SFP module emits CW light only. Using this setup, we compare the distributed sensing performance between "with data modulation" and "without data modulation" states, with the same configuration as in Figs. 2a-2f of the main text. The results for the two operating states are summarized in Supplementary Fig. 3.

When the test board works in mode 1, the resulting waterfall plot is shown in Supplementary Fig. 3a. Two stable vibration traces are visible at ~5 km and ~10 km, respectively. Zoom-in views of these regions are presented in Supplementary Figs. 3b and 3c: the 2-Hz vibration is localized to 9.78-9.80 km, and the 5-Hz vibration is localized to 4.88-4.90 km. The time-domain waveforms at these positions are plotted

in Supplementary Figs. 3d and 3e, with peak-to-peak phase variations of ~7×2π rad and ~3×2π rad, respectively, consistent with the results in Figs. 2e-2f of the main text.

When the test board works in mode 2, the SFP emits CW light only. The resulting waterfall plot is shown in Supplementary Fig. 3f and again displays vibration traces at ~5 km and ~10 km, respectively. Zoom-in views of these two positions are provided in Supplementary Figs. 3g and 3h, confirming that the vibrations remain confined within 9.78-9.80 km and 4.88-4.90 km. The time-domain waveforms (Supplementary Figs. 3i and 3j) closely match those obtained in mode 1 (Supplementary Figs. 3d and 3e).

Therefore, data modulation has no measurable impact on the sensing performance of H-DAS.

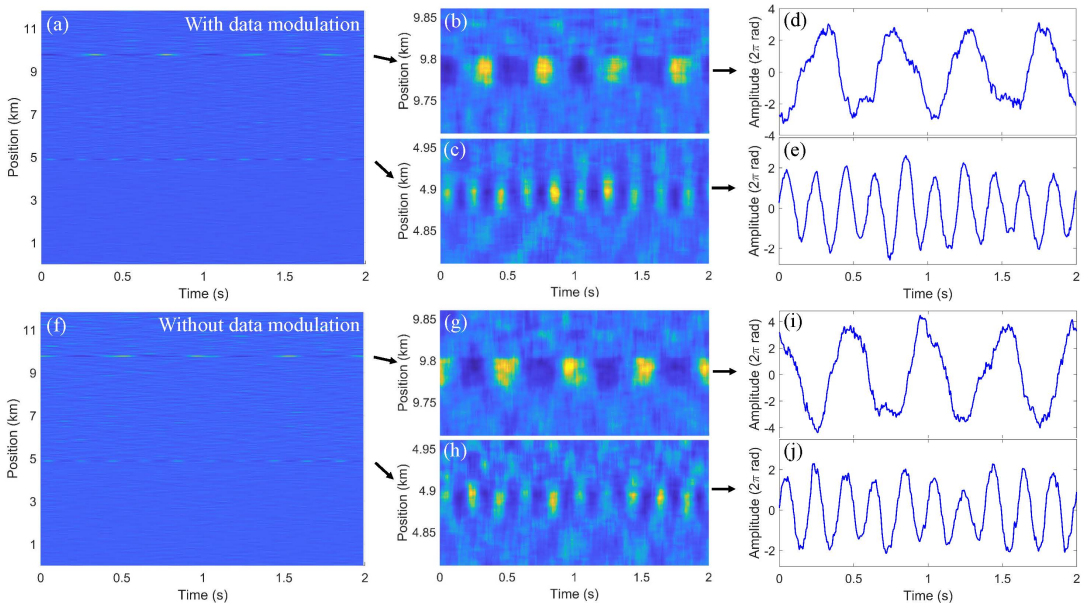

Supplementary Figure 3 | Comparison of distributed vibration sensing using the communication test board operated in two modes. a-e, Mode 1. **a,** Waterfall plot; **b,** zoom-in view of the 2 Hz vibration near 9.8 km; **c,** zoom-in view of the 5 Hz vibration near 4.9 km; **d,** time-domain waveform near 9.8 km; **e,** time-domain waveform near 4.9 km. **f-j,** Mode 2. **f,** Waterfall plot; **g,** zoom-in view of the 2 Hz vibration near 9.8 km; **h,** zoom-in view of the 5 Hz vibration near 4.9 km; **i,** time-domain phase waveform near 9.8 km; **j,** time-domain phase waveform near 4.9 km.

Supplementary Note 2: Sensing sensitivity of H-DAS system

The sensing sensitivity of the H-DAS system is evaluated under two configurations: an unmodulated CW output from a commercial optical communication test board, and data-modulated communication light from the commercial optical communication terminal used in the main text.

To evaluate the system sensitivity, we start from the demodulated optical phase change $\varphi(t,z)$ and convert it into strain perturbations $\varepsilon(t,z)$ over the gauge length $L_G = 5$ m. The phase change of the Rayleigh backscattered light and the strain integrated over L_G satisfy a linear relation[1], which can be written as:

$$\varepsilon(t,z) = \frac{\varphi(t,z)\cdot\lambda}{4\pi\zeta n L_G}, \tag{S1}$$

where n is the refractive index of the fiber, λ is the optical wavelength in vacuum, and ζ corresponds to a scalar multiplicative factor to account for changes in the index of refraction. We then estimate the strain power spectral density from $\varepsilon(t,z)$ and take the square root to obtain the strain amplitude spectral density, which quantifies the noise floor and sensitivity of the system. The spectra are calculated at a far-end position (z=11.82 km) and a near-end position (z=100 m), respectively.

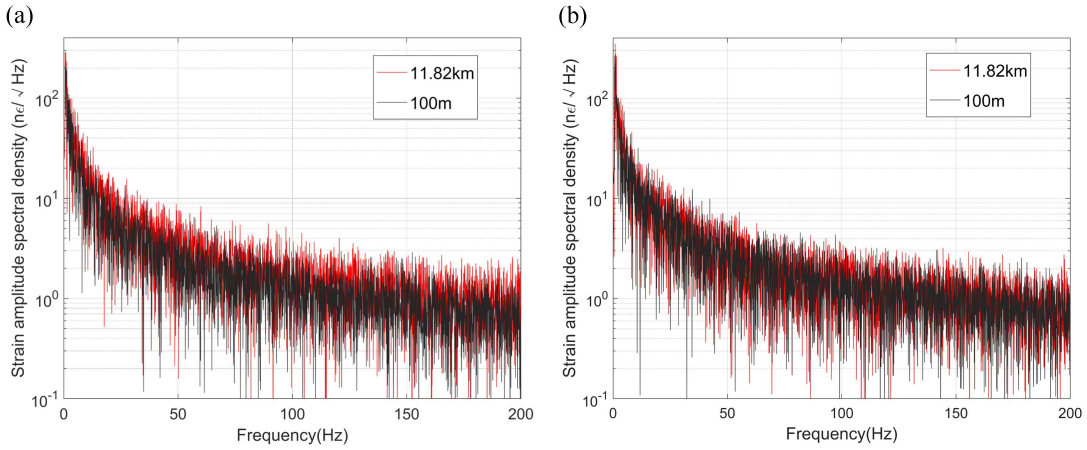

Supplementary Figure 4 | The sensing sensitivity of H-DAS system. a, Strain amplitude spectral density measured using an unmodulated CW output from a commercial optical communication test board. **b,** Strain amplitude spectral density measured using data-modulated communication light from the commercial optical communication terminal. Red curve: measurement result at 11.82 km.

Black curve: measurement result at 100 m.

The H-DAS sensitivity results using unmodulated CW light are shown in Supplementary Fig. 4a. The spectra measured at 11.82 km (red) and 100 m (black) exhibit similar shape and magnitude, corresponding to a sensitivity of ~2 nε/√Hz at 100 Hz and ~100 nε/√Hz at 1 Hz, which is comparable with the conventional DAS sensing sensitivity[2,3]. Supplementary Fig. 4b shows the H-DAS sensitivity results using the data-modulated communication light, where the spectral shape and magnitude remain essentially unchanged. These results indicate that data modulation has no measurable impact on the noise floor and the sensing sensitivity of the H-DAS system.

Supplementary Note 3: Field photographs of the construction site near the high-speed railway

Supplementary Figure 5 | Panoramic and close-up photographs of the construction site.

Supplementary Fig. 5 presents panoramic and close-up photographs of the construction site near the Yamenkou Bridge (the blue point in Fig. 5a). The central panoramic image indicates that the site is adjacent to the high-speed railway, forming an almost encircling layout around the line. The three photographs on the left correspond to the work area on the left side of the railway, where excavators, piling rigs, and numerous workers are visible. The three photographs on the right correspond to the work area on the right side of the railway, showing large material stockpiles and active material transport. Some stockpiles and operations are directly beneath the railway viaduct. Together, these images indicate the presence of heavy machinery and activities, which can generate strong vibrations and affect the nearby trackside fiber. These images further support our inference that the extra vibration event in Fig. 5d is attributable to construction activity.

Supplementary Note 4: Possible approaches to improve the H-DAS specification

Previous work on dual-comb–based coherently parallel DAS has demonstrated that the responses from different frequency channels can be linearly accumulated, with the sensing signal scaling with the number of comb lines. Using ten comb-line pairs, the study reported an approximately tenfold sensitivity enhancement compared to a single-frequency laser[4]. Commercial optical communication transmitters naturally provide "multi-channel" optical outputs (e.g., wavelength division multiplex), which can be exploited to optimize H-DAS. Specifically, different channels can be treated as parallel observations of the same distributed perturbation along the fiber link. Thus, one can average them. When the responses from different channels are consistent and the noises are approximately uncorrelated, the noise floor is expected to decrease by about $1/\sqrt{N}$, corresponding to a $\sqrt{N}$-fold improvement in sensitivity. Consequently, based on the natural architecture of the communication system, multi-channel average can serve as an effective approach to improve the sensitivity of H-DAS and, potentially, extend the sensing range.

Supplementary Reference

1. Ouellet, S. M. *et al.* Previously hidden landslide processes revealed using distributed acoustic sensing with nanostrain-rate sensitivity. *Nat. Commun.* **15**, 6239 (2024).
2. He, H. *et al.* Integrated sensing and communication in an optical fibre. *Light Sci. Appl.* **12**, 25 (2023).
3. Masoudi, A., Beresna, M. & Brambilla, G. 152 km-range single-ended distributed acoustic sensor based on inline optical amplification and a micromachined enhanced-backscattering fiber. *Opt. Lett.* **46**, 552–555 (2021).
4. Li, J. T. *et al*. Coherently parallel fiber-optic distributed acoustic sensing using dual Kerr soliton microcombs. *Sci. Adv.* **10**, eadf8666 (2024).